



Chitosan-iron oxide hybrid composite: mechanism of hexavalent chromium removal by central composite design and theoretical calculations

Pricila Maria Batista Chagas¹ · Aline Aparecida Caetano¹ · Marco Aurélio Rossi¹ · Mateus Aquino Gonçalves² · Teodorico de Castro Ramalho² · Angelita Duarte Corrêa³ · Iara do Rosário Guimarães¹

Received: 25 September 2018 / Accepted: 13 February 2019 / Published online: 8 April 2019

© Springer-Verlag GmbH Germany, part of Springer Nature 2019

Abstract

In this study, the synthesis of iron oxide stabilized by chitosan was carried out for the application and optimization in the removal process of aqueous Cr(VI) by central composite design (CCD). The calculation of these effects allowed to know, quantitatively, the variables and the interaction between them that could affect the Cr(VI) removal process. It was also verified that the most favorable conditions for chromium removal were the following: pH 5.0, Cr(VI) concentration of 130 mg L⁻¹, adsorbent mass of 5 mg, and Fe(II) content of 45% (w/w) in the CT-Fe beads. The adsorption kinetics performed under these conditions showed that the chitosan/iron hybrid composite is an adsorbent material with high chromium removal capacity (46.12 mg g⁻¹). It was found that all variables were statistically significant. However, it was observed that the variable that most affected Cr(VI) removal was the pH of the solution, followed by the concentration of chromium ions in solution and the interaction between them. Therefore, the studied experimental conditions are efficient in chromium adsorption, besides the operational simplicity coming from statistical design. Theoretical calculations showed that the most stable chitosan was that with Fe(II) in the structure, that is, in the reaction mechanism, there is no competition of Fe(II) with Cr(III, VI) in the available sites of chitosan. Thus, the theoretical calculations show that the proposed Cr(VI) removal is effective.

Keywords Cr(VI) adsorption · Central composite design · Theoretical calculations · Adsorption mechanism · Operational simplicity

Responsible editor: Tito Roberto Cadaval Jr

Electronic supplementary material The online version of this article (<https://doi.org/10.1007/s11356-019-04545-z>) contains supplementary material, which is available to authorized users.

✉ Iara do Rosário Guimarães
iaraguimaraes@dqi.ufla.br

- ¹ Laboratório de Catálise Ambiental e Novos Materiais, Departamento de Química, Universidade Federal de Lavras, CEP, Lavras, MG 37200-000, Brazil
- ² Laboratório de Análise Computacional, Departamento de Química, Universidade Federal de Lavras, CEP, Lavras, MG 37200-000, Brazil
- ³ Laboratório de Bioquímica, Departamento de Química, Universidade Federal de Lavras, CEP, Lavras, MG 37200-000, Brazil

Introduction

Chromium is one of the most toxic metals discharged into the environment by various industrial effluents and has become a serious health problem (Lee et al. 2017). As a hexavalent ion, this element does not have any essential metabolic function for plants and accumulates predominantly in the roots, inducing phytotoxicity and interfering in growth, nutrient absorption, and photosynthesis (Ashraf et al. 2017; Shahid et al. 2017). As a transition element, chromium can occur in different oxidation states. However, only Cr(III) and Cr(VI) are more stable, produced mainly from anthropogenic sources, such as industrial effluents from tanning, galvanizing, painting, and textile industries (Shahid et al. 2017). Cr(VI) has higher mobility in the soil, with toxicity about 10 to 100 times higher than Cr(III). For animals, the metal with oxidation state plus six has a mutagenic, carcinogenic, and teratogenic potential (Prado et al. 2016). Therefore, the efficient removal of

Cr(VI) from contaminated environments is a fundamental premise of technological development and industrial progress (Cunha et al. 2016; Ye et al. 2017).

In this context, adsorption appears as a recognized method, an efficient and economical way to remove contaminants in water bodies, due to its simplicity, reliability, and safety (Yao et al. 2014; Haldorai et al. 2015; Bibi et al. 2018). The modification of iron oxides with organic constituents has gained attention due to the obtention of materials with diverse structural properties and different applications. Iron oxide composites, particularly in the magnetite phase, have been exploited for the adsorption of organic and inorganic pollutants, mainly due to the rapid separation through the use of external magnetic fields (Hua et al. 2012; Rossi et al. 2014; Lingamdinne et al. 2017; Tahar et al. 2018).

The development of magnetic particles requires surface modification to improve the adsorption capacity for which they are intended. Iron oxides usually have a mass structure with reduced specific surface area, which negatively affects the adsorption process. Thus, researchers have been dedicated to reducing this type of problem associated with particle aggregation, by the hybridization of active constituents with other materials (Su 2017; Hao et al. 2016; Lu et al. 2017). The addition of organic compounds together with iron oxide in the Cr(VI) removal process may be advantageous to avoid the precipitation of the reduced chromium species, as it may be adsorbed on the organic matrix (Chagas et al. 2018). Therefore, the appropriate choice of the non-mineral constituent with specific functional groups can increase adsorption performance by the complexation mechanism and thus minimize the aggregating capacity of magnetite particles (Buerge and Hug 1999; Qin et al. 2016). Thus, oxygenated and nitrogenous groups are the main classes for the formation of coordinated structures based on Lewis acid-base chemistry. Chitosan is a low-cost biopolymer, renewable, and biodegradable, of great economic and environmental importance (Sahu et al. 2014; Choi et al. 2016). It has excellent metal adsorption properties, mainly due to the presence of amino ($-\text{NH}_2$) and hydroxyl ($-\text{OH}$) groups in its polymer matrix (Vieira et al. 2014).

Given the above, the synthesis of a material based on a highly dispersed iron oxide structure stabilized by chitosan (CT) was carried out in this study. The CT-Fe composite was formed by the direct incorporation of Fe(II) into the soluble carbohydrate gel. The polymer structure was regenerated for the production of nanostructured magnetic CT-Fe iron oxides with spherical shape. Chitosan beads, with different proportions of iron oxide, were tested for Cr(VI) removal in aqueous medium. Several papers currently available in the literature have already demonstrated the potential of CT in removing Cr. However, many of these manuscripts detail the experimental parameters in an individualized way, not taking into account its application in a real industrial process. In these situations, it is important to assume the effects of all variables and the

relations governing their mutual interactions. In this connection, Beheshti et al. (2016) published the effect of the independent variable and, since 2016, no other correlated study was found. Sikder et al. (2014) did not describe the integration of the altered physicochemical factors, even in later publications. This limitation is also found in other important studies (Kim et al. 2015; Yan et al. 2016; Li et al. 2013; Zhang et al. 2016). In this context, our research group published the first study that described and characterized more comprehensively the formation of the chitosan-iron oxide hybrid composite. This first study was also essential to know the behavior of the CT-Fe-Cr(VI) system since, only after the study of all the independent parameters, it was possible to define the minimum and maximum parameters with a higher confidence level for the optimization of the removal process of hexavalent chromium in a multivariate analysis (Chagas et al. 2018).

To develop a suitable adsorption process, there are a number of parameters that influence the process, such as pH, adsorbate concentration, adsorbent mass, and temperature, which should be studied. Thus, central composite design (CCD) was used to optimize all parameters that affect adsorption. In addition, for the surface chemistry of the process to be known in greater detail, it was assessed how independent parameters can at the same time interfere with the adsorption capacity of the system. This study succeeds the first experimental demand in which it was verified, in batch, which main parameters are responsible for interfering in the adsorption. Now, aware of this demand, CCD was used to reduce the total number of experiments in order to achieve the overall optimization of the combined process (Nunes et al. 2012; Bhatti et al. 2017). In this study, the effects of the following variables were investigated: iron content incorporated in the chitosan beads, pH of the reaction medium, adsorbent mass, and concentration of chromium ions in aqueous solution. In order to evaluate the reactions that occur in the system, theoretical calculations at the DFT level were also performed; 13 reactions of chitosan with iron(III) and chromium(VI) were proposed.

Material and methods

Experimental design for the optimization of multivariate parameters

In order to define the optimum aqueous Cr(VI) adsorption conditions, the parameters of iron mass content in the beads, adsorbent mass, pH, and concentration of Cr(VI) ions in solution were determined for the experimental design. For each parameter, the minimum and maximum levels of the study range were defined taking into account aspects such as feasibility and practicality of the process. Thus, the choice of Fe(II) contents in the range of 15–45% (w/w) was defined, since values above 50% (w/w) could compromise the physical

integrity of the beads; pH values of 5–9 represent the study range with the highest technical applicability, and the supernatant remaining after chromium removal would be within or adjacent to what is established by Resolution 357 of CONAMA (2011) and the World Health Organization (WHO) (2004); the adsorbent mass had values ranging from 20 to 50 mg (Sampaio et al. 2015) and, in relation to Cr(VI) concentration, the concentrations were in the range of 35–100 mg L⁻¹, since they are considered high above 100 mg L⁻¹ when toxic metals are removed and the limit of 35 mg L⁻¹ was chosen, once the CCD program is the optimization method used, allowing extrapolation to include axial points.

The analysis of the main effects and interactions that occurred on adsorption, with the variation of parameters in the selected range, was carried out by experimental design (central composite design, CCD). Twenty-seven tests were performed, considering the four defined variables, 15 factorial points, 8 axial points, and 3 central points (Table 1). The latter

were performed with the purpose of estimating the experimental error and the reproducibility of the obtained results. The Chemoface software, version 1.61 (Nunes et al. 2012), was used to design the experiments and optimize the adsorption process based on criteria of statistical significance.

The individual effects of the defined variables, as well as the effects of the interaction between these variables on the adsorption process, were calculated according to the methodology proposed by Neto et al. (2010). The significance of each effect was defined by direct comparison with the value of the critical effect, calculated in relation to the variation of repetitions at the central point (95% confidence interval), so that any effect that presented absolute value greater than the value calculated for the critical effect was considered significant for the process. The graphical representation of the analyses was performed with the construction of the Pareto chart.

In order to obtain the optimum conditions for the process and quantitative values for adsorption at any point within the

Table 1 Experimental design matrix of four variables with chrome removal response

Test	Content of Fe(II) (%) in the beads	pH	Adsorbent mass (mg)	Concentration of Cr(VI) in solution (mg L ⁻¹)	Removal of Cr(VI) <i>q_e</i> (mg g ⁻¹) ± SD
Variables	(<i>X</i> ₁)	(<i>X</i> ₂)	(<i>X</i> ₃)	(<i>X</i> ₄)	
1	15	5	20	35	6.55 ± 0.33
2	15	5	20	100	17.67 ± 0.56
3	15	5	50	35	2.85 ± 0.04
4	15	5	50	100	36.20 ± 0.67
5	15	9	20	35	7.40 ± 0.17
6	15	9	20	100	1.30 ± 0.11
7	15	9	50	35	3.30 ± 0.15
8	15	9	50	100	1.22 ± 0.17
9	45	5	20	35	1.99 ± 0.03
10	45	5	20	100	8.82 ± 0.01
11	45	5	50	35	20.55 ± 0.20
12	45	5	50	100	4.78 ± 0.05
13	45	9	20	35	10.22 ± 0.23
14	45	9	20	100	3.57 ± 0.11
15	45	9	50	35	6.17 ± 0.03
16	45	9	50	100	2.97 ± 0.05
17	0	7	35	67.5	5.00 ± 0.16
18	60	7	35	67.5	1.36 ± 0.12
19	30	3	35	67.5	5.17 ± 0.35
20	30	11	35	67.5	13.12 ± 0.12
21	30	7	5	67.5	2.08 ± 0.15
22	30	7	65	67.5	12.61 ± 1.15
23	30	7	35	2.5	3.16 ± 0.01
24	30	7	35	132.5	6.42 ± 0.30
25	30	7	35	67.5	4.26 ± 0.28
26	30	7	35	67.5	4.45 ± 0.03
27	30	7	35	67.5	4.38 ± 0.16

analyzed region, the experimental data were adjusted to a regression equation using the quadratic model, from which response surfaces were constructed for the range of studied values. The graphic construction was also enabled by the use of Chemoface software (Nunes et al. 2012).

Synthesis of chitosan and iron oxide beads stabilized by chitosan (CT-Fe)

The chitosan solution was prepared by solubilizing 3.5 g chitosan (CT) (low molecular weight, obtained from Sigma-Aldrich®, degree of deacetylation $80.7\% \pm 1.35$ (Chagas et al. 2015)) in 100 mL of acetic acid solution (2% v/v), under stirring for 1 h (Chagas et al. 2018). In this solution, different Fe(II) proportions were then incorporated in relation to the chitosan mass: (a) 0.525 g Fe(II) (CT-Fe 15% w/w); (b) 1.05 g Fe(II) (CT-Fe 30% w/w); (c) 1.575 g Fe(II) (CT-Fe 45% w/w); and (d) 2.10 g Fe(II) (CT-Fe 60% w/w), using the reagent $\text{FeCl}_2 \cdot 4\text{H}_2\text{O}$ (Fe contents were calculated by the CCD methodology, Table 1). The mixture remained under stirring until complete solubilization of this reagent.

For the production of the beads, the above mixture was dripped into a 2 mol L^{-1} NaOH solution using a needle attached to a syringe at a height of 10 cm from the solution, with the aid of a vacuum pump, immediately yielding gel coagulation in spherical shape. The pure chitosan solution was also dripped to obtain the polymer beads without the presence of the metal. The beads remained for 16 h in the base solution and were then washed with deionized water until neutral. Subsequently, the materials were oven dried at 60°C for 12 h (The dry bead had an average diameter of about 1.0 mm).

Characterization of materials

The morphological analysis of the materials was performed using a LEO 440 SEM equipment with an OXFORD detector, using a 15-kV electron beam. The functional groups of beads were determined by vibrational spectroscopy in the infrared region using Fourier transform. A Varian-660 IR, Pike, coupled to an ATR device with 32 scans and 4 cm^{-1} resolution, was used in the spectral range of $400\text{--}4000 \text{ cm}^{-1}$.

The procedure for calculating the zero charge point (pzc) consisted of adding 10 mg of the adsorbent in 10 mL of 0.1 mol L^{-1} aqueous KCl solution under 12 different initial pH conditions (1–12), adjusted with 0.1 mol L^{-1} HCl or NaOH solutions. After 24 h of contact to reach equilibrium and a thermostatic bath at 25°C under mechanical stirring, the solutions were filtered and the final pH was recorded (Prahas et al. 2008).

The nitrogen adsorption-desorption isotherms were obtained at 77K in a Quantachrome instrument (NOVA 1200). The samples were previously degassed for 12 h at 100°C . The

specific surface area was calculated using the BET equation. The pore size distribution and pore volume were calculated based on the N_2 adsorption isotherm, using the Horvath-Kawazoe (HK) method.

Removal tests of aqueous Cr(VI)

The experiments to select the most suitable Fe proportion in the chitosan beads for Cr(VI) removal were carried out in flasks containing 10 mL of the Cr(VI) ($\text{K}_2\text{Cr}_2\text{O}_7$) stock solution, together with the adsorbent materials (CT-Fe), kept under mechanical stirring for 24 h at $25^\circ\text{C} \pm 1^\circ\text{C}$ (the concentration of the solution, pH, and adsorbent mass were adjusted according to the CCD methodology). After adsorption, the residual chromium concentration in the solution was determined by the colorimetric method, using 1,5-diphenylcarbazide, and reading at the wavelength of maximum absorption of the formed complex, at $\lambda = 540 \text{ nm}$ (APHA 2012). Cr(total) was dosed after Cr oxidation in acidic medium with potassium permanganate at high temperature. Cr(III) was calculated by the difference between Cr(total) and Cr(VI) in the solution. Cr(VI) removal capacity was calculated using Eq. (1).

$$q_e \text{ (mg g}^{-1}\text{)} = \frac{C_0 - C_e}{m} \times V \quad (1)$$

where adsorption capacity $q_e \text{ (mg g}^{-1}\text{)}$ = adsorption capacity, $C_0 \text{ (mg L}^{-1}\text{)}$ = initial concentration content of Cr(VI) in the solution, and $C_e \text{ (mg L}^{-1}\text{)}$ = concentration of metal at equilibrium described in Eq. (1); $V \text{ (L)}$ = volume of sample solution and $m \text{ (g)}$ = adsorbent mass.

The kinetic study was conducted with the best conditions obtained by the optimization of the multivariate parameters by CCD.

Computational methods

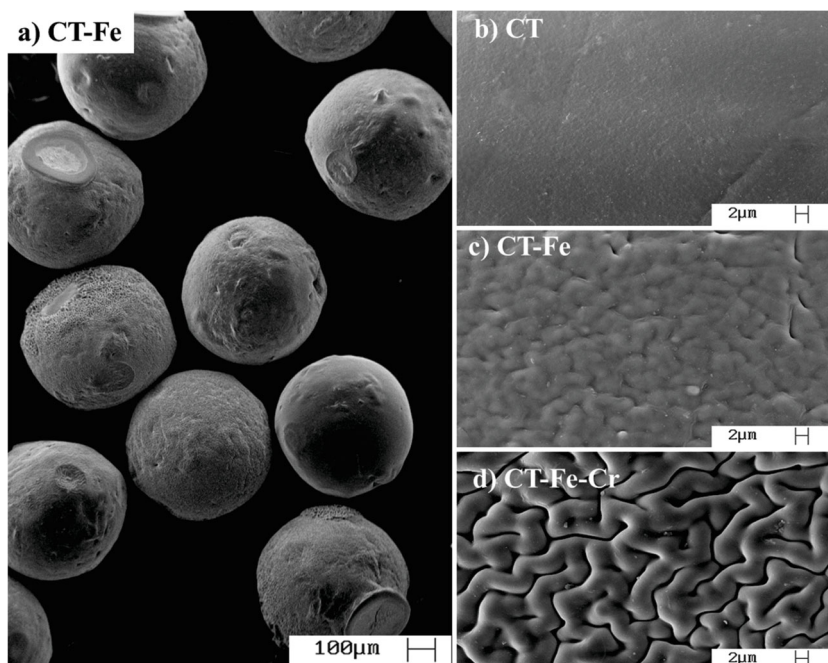
The structures were initially built in the Chemcraft program (Zhurko and Zhurko 2015). Subsequently, optimization and frequency were calculated with the ORCA program (Neese 2012), using the B3LYP functional and 6–31g basis functions for all atoms. Quantum theory of atoms in molecules (QTAIM) was calculated using the AIMALL package (Keith 2010) (they were calculated using QTAIMQB calculations; the results were analyzed by the AIMSTUDIO program, both are part of the AIMALL package).

Results and discussion

Characterization

Bead morphology was observed by scanning electron microscopy (Fig. 1). In Fig. 1a, it was observed that the CT-Fe

Fig. 1 Scanning electron microscopy (SEM). **a** Chitosan beads CT-Fe (45% w/w) (100 μm). **b** Chitosan (CT) (2 μm). **c** CT-Fe (45% w/w) (2 μm). **d** CT-Fe (45% w/w), after Cr(VI) removal (2 μm)



material (45% w/w) had a spherical shape and a homogeneous size. Pure chitosan displays a smooth and regular surface (Fig. 1b); the well-arranged polymer chains observed are probably a result of the functional groups present on its structure (–NH₂ and –OH).

In Fig. 1c, the composite material formed by iron oxide dispersed in the chitosan network (CT-Fe) is shown. Unlike the beads formed by pure CT, the addition of iron has a very pronounced effect on composite morphology, since the formed iron oxide gave the beads a highly rough and irregular surface in the form of folds. This morphological change observed in the material was possibly caused by the cross-linking of chitosan chains which, in the presence of iron, used –NH₂ and –OH groups to complex together with the metal. The highly rugged texture, with a modified surface arrangement, positively contributed so that adsorption events were optimized (Chagas et al. 2018).

After Cr(VI) adsorption on the beads, the surface was more strongly modified, which shows that the presence of the metal element was assertively responsible for disrupting the chitosan chains strongly bound by hydrogen bonds or any other cohesive force (dipole-dipole, dispersive forces, etc.) (Fig. 1d).

The values of the specific surface area (m² g⁻¹) of materials were calculated using the BET equation. The HK method was

used to calculate the corresponding pore size distribution (nm) and pore volume (cm³ g⁻¹). The results are presented in Table 2. The materials had an average pore size of 9.0 nm, which characterize them as mesoporous materials (Thommes et al. 2015).

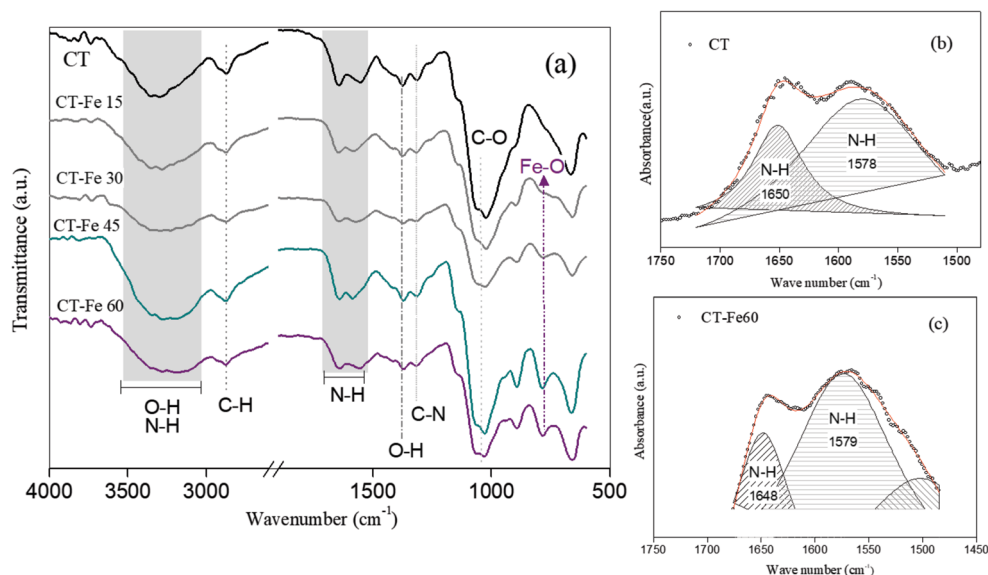
The iron oxide synthesized with chitosan led to an increase in surface area and pore volume, when compared to chitosan (Table 2). The high surface area value of the CT-Fe composite (1418.0 m² g⁻¹) is in agreement with the images obtained by scanning electron microscopy (Fig. 1b and c), in which a significant change in chitosan morphology was observed in the presence of the metal. This increase in the area associated with the rough appearance of the composite favors the adsorption processes, since the number of active sites available on the material surface also increases. Similarly, the adsorption of chromium ions by the CT-Fe composite reduced surface area (820 m² g⁻¹) and pore volume (0.127 cm³ g⁻¹), suggesting that the available active sites were occupied by the metal, reducing the contact surface and the adsorption of N₂.

The obtained results of the chitosan infrared spectroscopy (FTIR) analysis, CT-Fe (15, 30, 45, and 60% w/w), are shown in Fig. 2. For the pure polymer material, CT, the vibration broadband near 3000 to 3600 cm⁻¹ can be attributed to the O–H and N–H bonds present in its structure, as well as water

Table 2 BET surface area, average pore diameter, and total pore volume of CT, CT-Fe (45% w/w), and CT-FeCr

Sample	BET surface area (m ² g ⁻¹)	Average pore size (nm)	Pore volume (cm ³ g ⁻¹)
Chitosan	85.86	9.23	0.012
CT-Fe (45% w/w)	1418.0	9.24	0.215
CT-FeCr	820.0	9.68	0.127

Fig. 2 Infrared spectra of chitosan (CT) beads and CT-Fe (15, 30, 45, and 60% w/w) (a) and deconvolution of the overlapped bands (b, c)



on the surface of the materials. We also report the presence of bands at 1650 and 1590 cm^{-1} , related to the stretching of N–H amide bonds; this functional group is a remaining from the incomplete conversion of chitin to chitosan. Vibrations between 1420 and 1300 cm^{-1} represent the C–N bonding. Vibrations appearing on lower wavenumbers are characteristic of the deformations of C–O and C–N.

Changes were observed in the position and intensity of O–H and N–H vibration bands after the incorporation of Fe into the polymer matrix (CT-Fe 15, 30, 45, 60% w/w), as shown around 3000–3600 cm^{-1} and 1650–1590 cm^{-1} in Fig. 2. As described by Zhu et al. (2016), the deconvolution analysis is an effective way to find hidden peaks and can distinguish groups located in different positions. The deconvoluted N–H regions of the IR spectra are shown in Fig. 2b and c for CT and CT-Fe materials. The components of amino groups are obtained by Lorentzian fits. From the mathematical adjustment performed for the bands corresponding to symmetrical angular deformation N–H (1650 and 1590 cm^{-1}) for CT and CT-Fe 60%, it is possible to show the displacement of this band to regions of lower intensity with the presence of Fe in the polymer matrix, for example, at 1650 cm^{-1} for CT and at 1648 cm^{-1} for CT-Fe 60% (positions and assignments of these peaks, as well as full widths at half maximum, FWHM) (Branca et al. 2016). This behavior can be explained by chemical factors that affect vibrational aspects (Wang and Liu 2014). Side effects such as the neighborhood of a functional group become significant when the neighborhood exhibits strong receptor or electron donor characteristics. Iron (Fe) is an electron acceptor acting as a Lewis acid and, consequently, this characteristic will affect the bond strength and the dipole moment of the –NH group (Pasquini 2003). Since the functional groups –NH or –OH have strong bonds (hydrogen bonding) on their structure, the bands shift to a higher

wavenumber. Since the now-complexed Fe atom is located near the bonding site, this bond will be weakened, causing changes in the electron density distribution and the bands move to regions of lower intensity. In addition, the presence of an electron acceptor might cause the hydrogen bonding bands to become more harmonic with reduced intensity (Rakkapao et al. 2011; Singh and Ahmad 2010).

Another side effect at the microscopic level is the material crystallinity. After Fe incorporation, the composites become more amorphous in relation to the semi-crystalline nature of the polymer, which causes a reduction in the bands related to the polymer (Pasquini 2003).

For CT-Fe materials, it was observed that, in addition to the bands characteristic of the polymer, a new band also appears in low-frequency regions, at 789 cm^{-1} . This band begins to appear in the CT-Fe material (30% w/w) and is more evident with the increase in Fe incorporated into chitosan (CT-Fe 45 and 60% w/w). According to Cornell and Schuwertmann (2003), this band is compatible with Fe–O vibrations in structures whose crystalline arrangement is related to the three-dimensional network of oxides, confirming the formation of the active phase directly bound to the chitosan matrix (Beheshti et al. 2016).

Optimization of multivariate parameters in the removal of aqueous Cr(VI)

The optimization step consisted in obtaining the best analysis response with the investigation of important variables and their interactions using a second-order model. CCD was used for the optimization of the analysis methodology of aqueous Cr(VI) removal by the CT-Fe hybrid composite against the parameters: Fe(II) content in the beads, pH, adsorbent mass, and concentration of chromium ions in solution. Table 1

shows the removal of aqueous Cr(VI) against the parameters and their respective levels evaluated.

After obtaining the experimental results, the effect of the variables and their interactions on the removal of aqueous Cr(VI) were statistically estimated and the results are presented in the Pareto chart (Fig. 3). The objective of the Pareto chart is to graphically demonstrate the significance and the relationship of the effects of the variation in the studied parameters on the adsorption process. The dotted line is related to the value of *p*; the variables or interactions that exceed this line are those that represent significant effects on the response variable, that is, the removal capacity of Cr(VI).

It was possible to establish that the parameter whose variation most influenced the adsorption results was pH, with an antagonistic effect (negative signal), so that higher adsorption rates will be obtained in acidic medium. After pH, the second most important parameter to be taken into account in the search for optimization was the concentration of chromium ions in solution, with a synergistic effect (positive signal), in which higher removal values were obtained in more concentrated metal solutions.

According to the Pareto chart, the third parameter that was significant involves the catalyst mass. In this case, smaller masses reflect in an increase in Cr(VI) removal capacity. Among the defined parameters, the change in Fe(II) content in the beads was less significant for the removal process of chromium ions, showing a synergistic effect (positive signal), so that higher iron oxide contents in the chitosan matrix lead to greater removal capacity.

As important as the analysis of the main effects of each parameter, it was also possible to observe the effects that may arise from the interaction between them (Fig. 3), when there is a simultaneous variation in their levels. Basically, a significant interaction effect leads to the conclusion that there

will not be only a single optimized value when varying the other parameters. In this study, the effects of the simultaneous variation in pH and concentration of chromium ions ($X_2 * X_4$), as well as pH and composite mass ($X_2 * X_3$), had a greater interference in the removal values than the individual variation of the iron content in the chitosan matrix, which was also significant, but to a lesser extent.

The interaction between iron content and pH ($X_1 * X_2$), as well as the interactions between iron content and composite mass ($X_1 * X_3$), was not significant. This indicates that the optimum value of the iron content incorporated in the beads will undergo a negligible variation in the different pH values and composite masses. Therefore, the process was favored in any incorporated Fe content (15, 30, 45, and 60% w/w), due to its synergistic chitosan/iron effect.

As for most of the effects, a significant interaction occurred in order to analyze the theoretical prediction of the optimum condition at each point within the analyzed range; the construction of the response surface is very important, once it reveals which value of a given parameter will be the ideal and significant as a function of the interactions with other parameters.

The construction of the response surface is given by the regression equation that allows the theoretical prediction of the adsorption values at any point within the limits defined for each parameter in the minimum and maximum levels. For the adsorption study of chromium ions in solution by the composite under different conditions, the regression equation was obtained by quadratic adjustment, with $R^2 = 0.9666$, $F = 24.8312$, and probability of 1.0717×10^{-6} .

In general, good adjustments are obtained when the R^2 value is close to 1, which occurred in this study, in addition to the high value of the *F* test, evidencing that most of the variance in the response was adequately accounted for by the

Fig. 3 Pareto chart for the study of the effects of the variation in the parameters on the aqueous Cr(VI) adsorption process

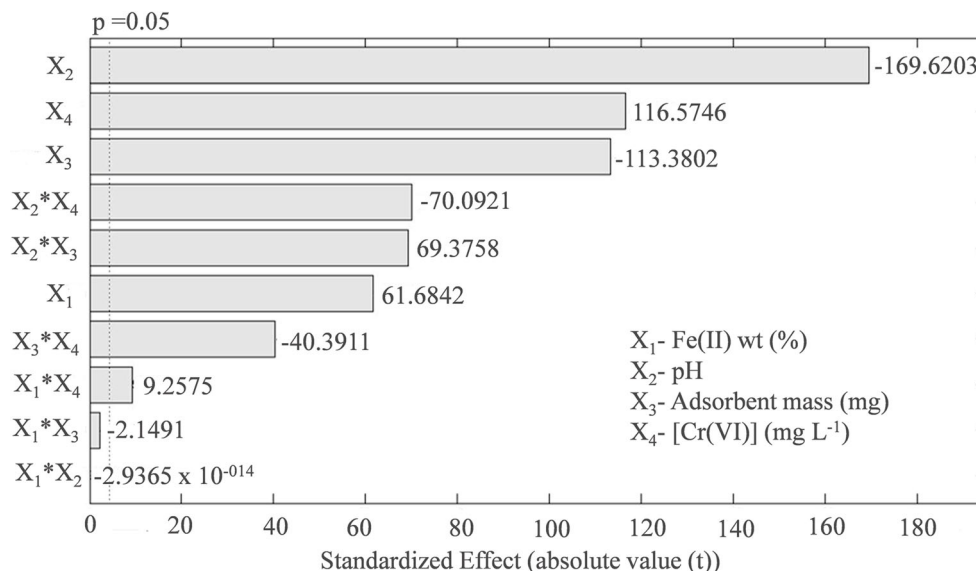


Table 3 Coefficients and significance tests of the variables obtained for chromium adsorption

Parameters	Coefficients (<i>B</i>)	Error	<i>t</i>	<i>p</i>	Significance
Constant (<i>B</i> ₀)	27.81	0.4869	57.12	3.064×10^{-4}	Yes
<i>X</i> ₁	0.086	0.0089	9.639	0.0106	Yes
<i>X</i> ₂	-5.140	0.0811	-63.35	2.491×10^{-4}	Yes
<i>X</i> ₃	-0.6970	0.0093	-75.18	1.770×10^{-4}	Yes
<i>X</i> ₄	0.2968	0.0041	71.58	1.951×10^{-4}	Yes
(<i>X</i> ₁) ²	-5.194×10^{-4}	8.731×10^{-5}	-5.949	0.0271	Yes
(<i>X</i> ₂) ²	0.2417	0.0049	49.22	4.126×10^{-4}	Yes
(<i>X</i> ₃) ²	0.0046	8.731×10^{-5}	52.84	3.579×10^{-4}	Yes
(<i>X</i> ₄) ²	-4.675×10^{-5}	1.860×10^{-5}	-2.513	0.1285	No
<i>X</i> ₁ <i>X</i> ₂	-2.116×10^{-16}	7.561×10^{-4}	-2.798×10^{-13}	1.000	No
<i>X</i> ₁ <i>X</i> ₃	-2.167×10^{-4}	1.008×10^{-4}	-2.149	0.1646	No
<i>X</i> ₁ <i>X</i> ₄	4.308×10^{-4}	4.653×10^{-5}	9.257	0.0115	Yes
<i>X</i> ₂ <i>X</i> ₃	0.0525	7.561×10^{-4}	69.38	2.077×10^{-4}	Yes
<i>X</i> ₂ <i>X</i> ₄	-0.0245	3.490×10^{-4}	-70.09	2.035×10^{-4}	Yes
<i>X</i> ₃ <i>X</i> ₄	-0.0019	4.653×10^{-5}	-40.39	6.124×10^{-4}	Yes

*X*₁ = content of Fe(II)% in the beads, *X*₂ = pH, *X*₃ = adsorbent mass (mg), *X*₄ = concentration of Cr(VI) ions in solution (mg L⁻¹)

adjustment performed by the quadratic model. In addition, probability values below 0.05 determine a successful fit at a 95% confidence interval, confirming the reliability of the fit since the value was in the order of 10⁻⁶ (Table S1 in the Supplementary Material). The coefficients of the regression equation, as well as their level of significance, are presented in Table 3.

The regression equation (Eq. (2)), therefore, was:

$$Y = 27.8076 + 0.0858X_1 - 5.1398X_2 - 0.6968X_3 + 0.2968X_4 - 5.1944 \times 10^{-4}(X_1)^2 + 0.2417(X_2)^2 + 0.0046(X_3)^2 + 4.3077 \times 10^{-4}X_1X_4 + 0.0525X_2X_3 - 0.0245X_2X_4 - 0.0019X_3X_4 \quad (2)$$

where the term *Y* is the removal capacity of Cr(VI) (*q_e* (mg g⁻¹)) by the beads. In the generated equation, the coefficients related to the square of the concentration of chromium ions in solution (*X*₄), as well as those related to the interaction effects between iron content and pH (*X*₁*X*₂), iron content and composite mass (*X*₁*X*₃), were disregarded, since they were not significant (Table 3).

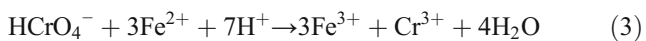
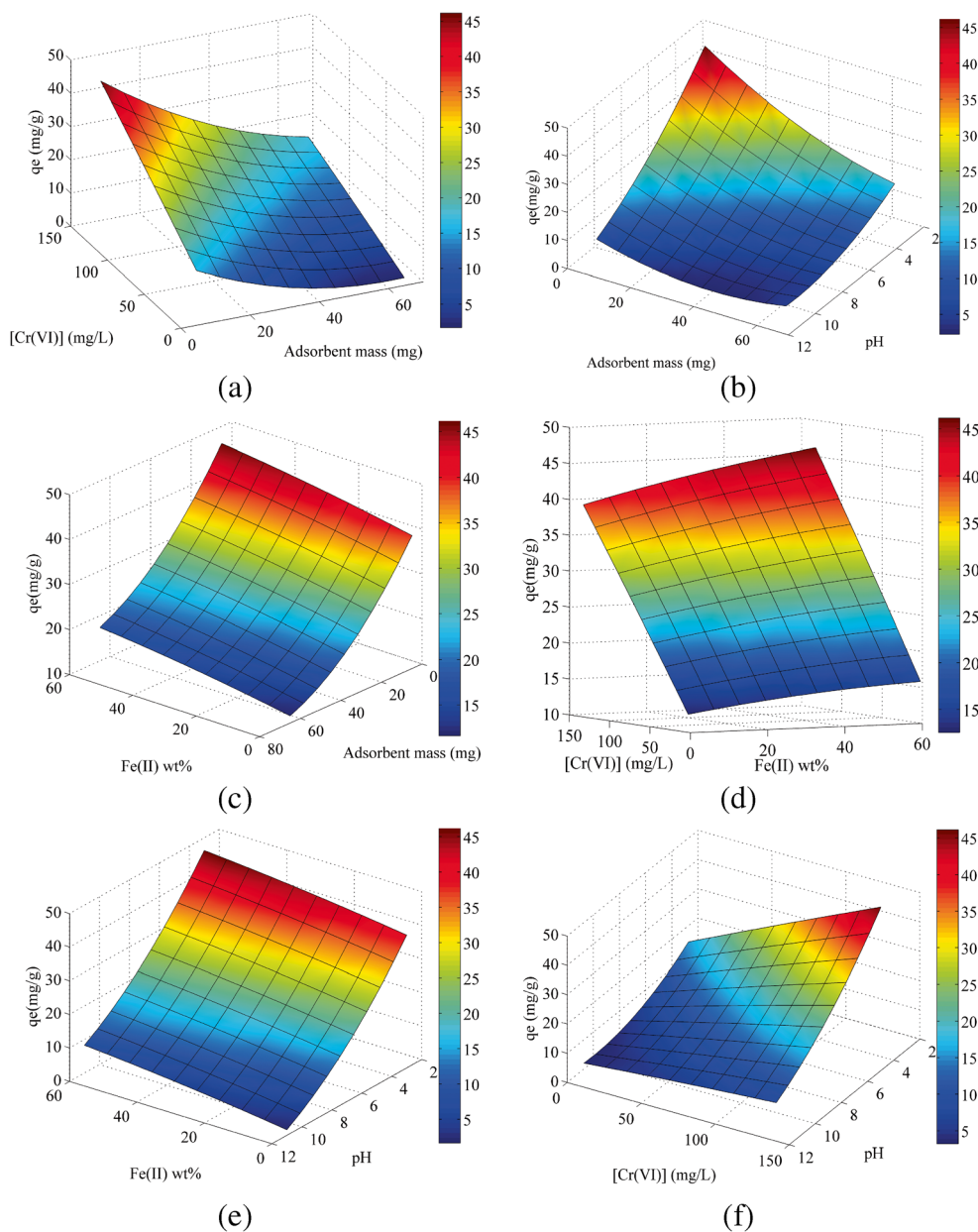
With the generated equation, surface response graphs were plotted, and are presented in Fig. 4. Six 3D graphs were constructed, showing the effects of the variables (*X* and *Y* axes) for the obtained area (*Z* axis) on the removal capacity of aqueous Cr(VI).

Figure 4a shows the response surface for the interaction between adsorbent mass (5–100 mg) and the increase in the concentration of Cr(VI) ions in solution (2.5–100 mg L⁻¹). In this study, it was possible to observe that the smaller amount of adsorbent (5 mg) has a greater removal capacity in milligrams of Cr per gram of adsorbent. This effect was also observed in Fig. 4b and c: interaction of adsorbent mass with pH and

increase in iron content in chitosan. In general, an increasing mass increases the removal efficiency in percentage, which is related to the greater number of binding sites; however, this value in percentage frequently leads to wrong adsorption values, since it does not take into account the mass and the volume, and is best expressed by the removal capacity *q_e*, expressed in milligrams per gram. With a strong theoretical basis that justifies the use of the *q_e* component in detriment to the percentage of metal removal, the results of the response surfaces are consistent with those obtained by adjustments to the adsorption isotherm models (Wibowo et al. 2017; Shekari et al. 2017), with the chemical viability of the former corroborating the latter. In addition, it is possible to mention the tendency of the literature that points to the use of data expressed as adsorbent accumulation capacity (Bhatti et al. 2017; Wu et al. 2017). Finally, it can be considered that the removal capacity of aqueous Cr(VI) will be much greater, the smaller the amount of CT-Fe composites, which makes the adsorption process feasible for practical and economic purposes.

According to the analysis of the response surfaces, as the proportion of Fe(II) (15, 30, 45, and 60% w/w) in relation to chitosan mass was increased, a higher removal capacity of aqueous Cr(VI) was obtained (Fig. 4c–e). The formation of iron oxide in the chitosan matrix improves the removal of chromium ions, since the creation of metallic active sites on the surface of the polysaccharide facilitates the reduction of Cr(VI) to Cr(III) (Eq. (3)). In addition, the simultaneous effect between the metal and the organic compound is reported, both of which may be involved in Cr(VI) reduction. Fe(II) potentiates the reduction kinetics, while the organic binder participates in the adsorption of the reduced species (Buerge and Hug 1999; Qin et al. 2016).

Fig. 4 Response surface obtained by adjusting the data with the quadratic model and influence of the parameters in the adsorption process. **a** Concentration of chromium ions and adsorbent mass. **b** pH and adsorbent mass. **c** Fe(II) content in chitosan (CT) beads and adsorbent mass. **d** Concentration of chromium ions and Fe(II) content in CT beads. **e** pH and Fe(II) content in CT beads. **f** Concentration of chromium ions and pH



However, the increase in iron incorporated in the beads was the parameter that had the least influence on chromium removal. This suggests that the adsorption process is favorable with any iron content incorporated in the beads.

The proposed optimization method by CCD in the removal of aqueous Cr(VI) was successful, since the most important parameter in the evaluation of adsorbent capacity was pH, once it affected both metal ion speciation in the solution and the nature of the adsorbent, especially with the protonation/deprotonation of the functional groups present on the surface. In this study, the removal capacity of Cr(VI) was higher in

acidic medium (Fig. 4b, e, f) and, to better understand the results, it was necessary to analyze chromium speciation and adsorbent surface.

The relative distribution of Cr(VI) species in solution is dependent on pH and concentration of Cr(VI) in solution. At pH 1, chromium exists as chromic acid (H_2CrO_4) whereas, in a pH range of 1–6, different forms of chromium coexist, such as dichromate ($\text{Cr}_2\text{O}_7^{2-}$) and hydrogen chromate (HCrO_4^-), whose latter is predominant; on the other hand, for values greater than 6, chromate (CrO_4^{2-}) prevails. $\text{Cr}_2\text{O}_7^{2-}$ ions occur when the concentration of Cr(VI) goes beyond 1 g L^{-1} (Dinker and Kulkarni 2015). Therefore, in this study, the predominant species were HCrO_4^- and CrO_4^{2-} .

In order to analyze the charge of the functional groups distributed on CT-Fe structure, the point of zero charge (pzc) was calculated for the pure chitosan (CT) and CT-Fe (Chagas et al. 2018).

The calculated values of pzc for both CT (7.02) and CT-Fe (6.98) were very similar to each other (Figure S1, Supplementary Material). Therefore, it is possible to infer that at pH values below the pzc, the functional groups present in CT and CT-Fe will display a positive net charge. The $-NH_2$ and $-OH$ groups, found in both polymers structures, will be completely protonated $-NH_3^+$ and $-OH_2^+$. As for the CT-Fe, the $FeOH_2^+$ rich surface sites will be able to attract the negatively charged Cr(VI) ions present in the solution in the form of $HCrO_4^-$, resulting in a greater Cr(VI) removal in acidic medium. In addition, it may occur parallel or later to the electrostatic process in which the Cr(VI) is attracted to the surface of the material, the reaction described by Eq. (3). According to this equation, H^+ ions are required and consumed during the reaction (Lv et al. 2011; Xiao et al. 2013). H^+ and Fe(II) may favor the reduction from Cr(VI) to Cr(III). Once reduced to the trivalent form, Cr(III) ions are adsorbed in the organic matrix; in this case, there is the formation of the covalent bond $-H_2N-Cr(III)$, by the non-binding electrons of nitrogen, in a specific coordinate bond (Chagas et al. 2018).

However, the decrease in adsorption capacity at higher pH can be explained both by the competition of $HCrO_4^-$ and HO^- anions available in the medium to be adsorbed on the surfaces of the solid (Yao et al. 2014), and by the decrease in the number of positively charged sites that are no longer formed with increasing pH of the medium.

Another important parameter evaluated by response surface analysis was the high removal capacity of CT-Fe composites in relation to the high concentration of chromium ions in solution (Fig. 4a, d, f). Thus, the best conditions for the adsorption of chromium ions against the optimized parameters were 5 mg of the CT-Fe composite (60% w/w) in 130 mg L^{-1} Cr(VI) solution and in acidic medium (considering pH 5.0 ideal, since it represents the pH of the 130 mg L^{-1} solution without adjusting this parameter, which makes the adsorption process viable). Thus, the kinetic study was conducted under these conditions, except for the iron content in the beads, which was 45% (w/w), due to the fact that contents of 60% (w/w) could compromise the physical integrity of the beads. In addition, the adsorption process proved to be favorable at any iron content incorporated.

Kinetic study

The adsorption kinetic (Fig. 5) shows the effect of contact time on Cr(VI) removal in CT-Fe beads (45% w/w). As can be perceived, there was a fast exponential adsorption rate, reaching to a maximum within 60 min of contact between the adsorbent and adsorbate. To understand the adsorption

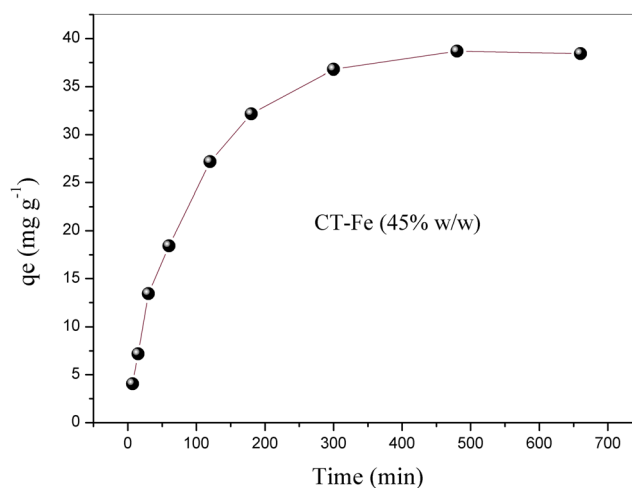


Fig. 5 Effect of contact time on Cr(VI) removal in CT-Fe beads (45% w/w) (5 mg adsorbent; 10 mL of 130 mg L^{-1} Cr(VI) solution at pH 5.0, temperature $25\text{ }^\circ\text{C}$)

mechanism, the nonlinear kinetic models including pseudo-first-order, pseudo-second-order, Weber-Morris (intraparticle diffusion), Boyd, and double-exponential models were applied. The parameters obtained by each model are shown in Table 4, and the graphs can be consulted in the Supplementary Material section (Figure S2–S5).

The best fit of the experimental data was expressed by the comparison of the coefficient of determination (R^2). All these statistical parameters were calculated using the software OriginPro 8.0 (graphing and data analysis software). The best adjustment of the experimental data was expressed by the comparison of the coefficient of determination (R^2), standard deviation (SD), the sum of squared errors of prediction (SSE), and chi-squared (χ^2) (Simonin 2016).

The pseudo-second-order kinetic model was the one that provided better adjustments in relation to pseudo-first-order (Figure S2, Supplementary Material), suggesting the presence of chemical interactions. The CT-Fe material (45% w/w) showed a high Cr(VI) removal capacity of 46.12 mg g^{-1} , which is much higher than those shown in Table 1, indicating that the experimental conditions by CCD, when optimized and applied at the same time, potentiated the adsorption process, increasing the kinetic adsorption capacity of the material. As for Fig. 4, it is observed that the value of the maximum adsorption capacity obtained by the pseudo-second model at equilibrium is similar to the values obtained by the CCD software.

The good fit to the pseudo-second-order model suggests chemical adsorption as a limiting step, and not mass transfer, in the early stages of the process (Sen Gupta and Bhattacharyya 2011). The pseudo-second-order model suggests that two processes are occurring in series or in parallel, one faster, causing the equilibrium to be reached quickly, and one slower, which can continue for a long period of time. This suggests that Cr(VI) removal possibly occurs in two stages: the electrostatic attraction of chromium ions and subsequently

the reduction of Cr(VI), and the reduced form is probably adsorbed by the formation of the covalent bond –H₂N–Cr(III).

The intraparticle diffusion curve can include several straight-line sections, with each section corresponding to a step of the adsorption process (Weber and Morris 1963; Bozorgi et al. 2018). The Morris-Weber model for the removal of Cr(VI) in the CT-Fe beads reflects on a graph with two linear portions, distinguishing 2 stages of adsorption (Figure S3, Supplementary Material), which corroborates with the pseudo-second-order kinetic model. The first stage, accounting for most of the adsorption, represents the gradual adsorption on the adsorbent surface, while the second stage represents the slow equilibrium phase, when Cr occupies all the active sites in the adsorbent and the maximum adsorption is reached (Bozorgi et al. 2018), which is in agreement with the data presented in the BET area analysis (Table 2). These steps may correspond to the electrostatic approximation of the anionic chromium form (HCrO₄⁻) after its reduction. The second stage corresponds to the adsorption of Cr(III) ions by the

surface functional groups of the material. According to the value of C_i (-2.31), intraparticle diffusion is involved in the adsorption process, but is not the only mechanism responsible for governing the adsorption rate (Madala et al. 2017).

The Boyd model is applied to check whether sorption proceeds via film diffusion or intraparticle diffusion mechanism. Film diffusion is the transport of adsorbents to the outer surface of the adsorbent, while particle diffusion is the transport of adsorbents into the pores of the adsorbent (Boyd et al. 1947). The plots of B_t vs t at different initial removal concentrations of Cr(VI) are shown in Supplementary Figure S4, which are linear with the correlation coefficient (R²) greater than 0.996.

According to the Boyd model, if the linear graph passes through the origin, the diffusion is controlled by particle diffusion; otherwise, it is controlled by film diffusion. As all Boyd plots intercept values did not pass through zero, diffusion can be controlled by film diffusion or in combination with other mechanisms (Madala et al. 2017). Therefore, the

Table 4 Kinetic adsorption parameters calculated by kinetic models nonlinear regression analysis

Kinetics models	Parameters	CT-Fe (45% w/w)	
Pseudo-first-order model	k_1 (min ⁻¹)	0.114	
$q_t = q_e (1 - e^{-k_1 t})$	q_e (mg g ⁻¹) ± SD	38.01 ± 1.81	
	R ²	0.985	
	χ ²	1.46	
	SSE (%)	5.86	
Pseudo-second-order model	k_2 (g mg ⁻¹ min ⁻¹)	0.030	
$q_t = \frac{K_2 q_e^2 t}{1 + K_2 q_e t}$	q_e (mg g ⁻¹) ± SD	46.12 ± 2.46	
	R ²	0.995	
	χ ²	0.685	
	SSE (%)	2.74	
Intraparticle diffusion model	Stage I		
	$q_t = k_{id} t^{1/2} + C$	k_{id} (mg g ⁻¹ min ^{-1/2})	2.63
		C _i (mg g ⁻¹)	-2.30
		R ²	0.992
	Stage II		
	k_{id} (mg g ⁻¹ min ^{-1/2})	k_{id} (mg g ⁻¹ min ^{-1/2})	0.020
C _i (mg g ⁻¹) ± SD		33.60	
R ²		0.379	
Boyd model	Slope	0.009	
$B_t = -0.4977 - \ln(1 - F)$ $F = q_t/q_e$	Intercept	-0.415	
	R ²	0.996	
Double-exponential model	q_e (mg g ⁻¹) ± SD	38.92 ± 0.05	
$q_t = q_e \frac{D_1}{m_{ads}} \exp(-k_{D1} t) - \frac{D_2}{m_{ads}} \exp(-k_{D2} t)$	D ₁ (g L ⁻¹)	0.003	
	D ₂ (g L ⁻¹)	0.017	
	k _{D1} (min ⁻¹)	0.091	
	k _{D2} (min ⁻¹)	0.009	
	SSE (%)	0.168	
	R ²	0.998	

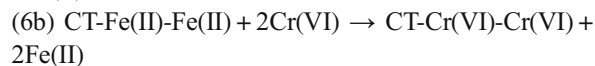
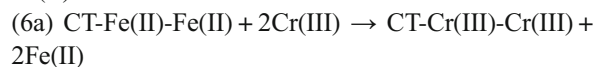
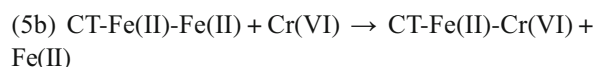
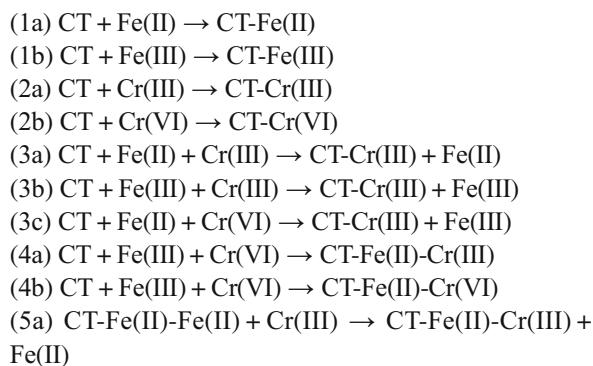
phase that governs the adsorption process in this study is probably the electrostatic attraction of the anionic species of chromium in solution, and the reduced chromium is adsorbed on the surface of the CT-Fe beads.

The double-exponential function is used here to describe a two-step adsorption mechanism controlled by diffusion: transport of the metal ion to the external surface of the adsorbent as a rapid phase and adsorption of the metal ion on the inside surface of the adsorbent as a slow phase (Talebi et al. 2017; Tehrani et al. 2017; Bozorgi et al. 2018). Among the five models applied to help understand kinetic behavior, the double-exponential model had the highest degrees of freedom and presented the greater R^2 (0.998) and lowest SSE (0.168%), indicating better consistency with the experimental data (Figure S5, Supplementary Material). The parameters D_1 and D_2 (g L^{-1}) are rate constants of the rapid and slow steps for chromium adsorption, respectively; k_{D1} and k_{D2} (min^{-1}) are constants controlling the mechanism and m_{ads} (g L^{-1}) is the adsorbent concentration. In this model, the sum of D_1/m_{ads} (5.84 mg g^{-1}) and D_2/m_{ads} (33.08 mg g^{-1}) has the same physical significance as the calculated value of q_e (Table 4). The $k_{D1} > k_{D2}$, during the first step, a rapid metal uptake takes place, involving external and internal diffusion. Subsequently, a slow step prevails; the intraparticle diffusion controls the adsorption rate and finally the metal uptake reaches equilibrium (Chiron et al. 2003). Therefore, the adsorption process was characterized by the presence of the anionic form (HCrO_4^-) on the outer surface of the adsorbent CT-Fe (electrostatic attraction by functional groups NH_3^+ and $-\text{OH}_2^+$) and the second step is chromium reduction and its adsorption by chemical bonds ($-\text{H}_2\text{N}-\text{Cr(III)}$).

Computational studies

Thermodynamic study of chitosan

In order to verify the reaction of chitosan with iron and chromium (III, VI), proposals were made, based on theoretical calculations of the standard Gibbs free energy (ΔG^0). The reaction proposals are as follows:



In order to know which reaction is most favorable to occur, ΔG^0 was calculated for each proposal Eq. (4). Below, the description of the calculations used in proposal 1. It is important to emphasize that similar calculations were made for the other proposals and the results are shown in Table 5.

$$\Delta G^0 = G_{\text{chitosan-Fe}} - (G_{\text{chitosan}} + G_{\text{Fe}}) \quad (4)$$

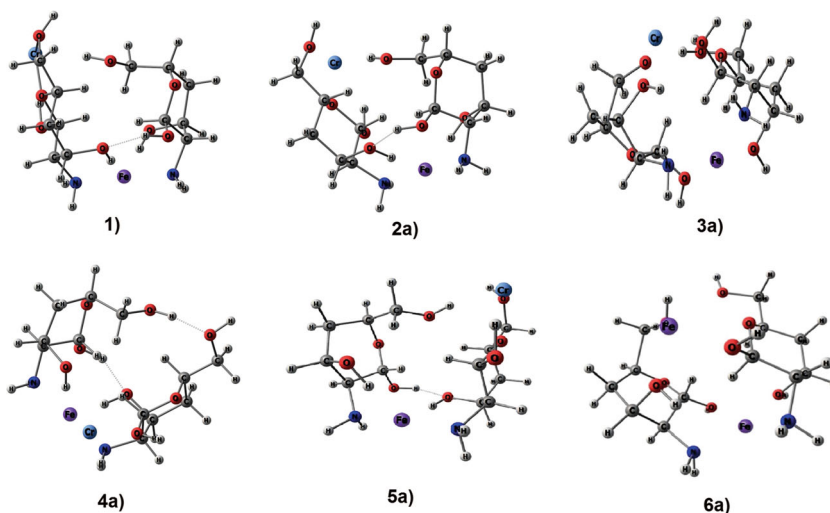
About 13 proposals were presented and it was observed that proposals 3a and 3b obtained ΔG^0 lower than others, that is, it is the most stable proposal. By theoretical calculations of ΔG^0 , the chitosan structure is more stable with respect to Fe(III) atoms than Fe(II) atoms. Regarding the structural characteristics of the polymers and their reaction sites, the stability constants of complexes formed by $-\text{OH}$ groups and metal ions have lower values, when compared to the stability constants of amino groups (Gyliene et al. 2014). It could be suspected that a part of the rapid conversion of Fe(II) to Fe(III) proceeds in most of the solution or even directly on the surface of chitosan. The stability of complexes and reactions of coordination compounds depends on the experimental values of the formation constant, but the charges and the radius of atoms can be used for stability predictions; in this case, Fe(III) has a higher value of charge/radius than Fe(II), which results in the formation of more stable complexes.

By theoretical calculations of ΔG^0 is possible to observe that the chitosan structure is more stable with the Fe(II) atom than with the Cr(III, VI) atom. Thus, it is believed that there is

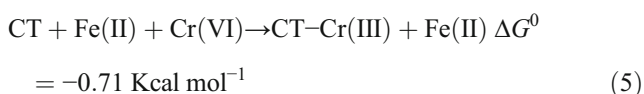
Table 5 Results of ΔG^0 for the proposed reactions

Proposals	ΔG^0 (Kcal mol ⁻¹)
1a	-0.60
1b	-0.74
2a	-0.59
2b	+0.28
3a	-137.15
3b	-152.42
3c	-136.14
4a	-129.48
4b	-129.40
5a	-119.10
5b	-108.42
6a	-28.08
6b	-20.78

Fig. 6 Structures of optimized geometries for the proposals



no competition between Fe(II) and Cr(III, VI); therefore, the chromium atom will occupy other available sites of the chitosan structure and not replace Fe(II) atoms (Fig. 6). It is also interesting to note that the structures with Cr(VI) were less stable in relation to Cr(III); thus, the Cr(VI) removal proposal is effective, following the reaction Eq. (5):



The Cr(VI) removal mechanism by CT-Fe beads first involves the electrostatic attraction of the anionic Cr(VI) forms through the CT-Fe beads; Cr(VI) is then reduced by Fe(II) and Cr(III) adsorption occurs by strong interactions, possibly by the formation of the covalent bond $\text{-H}_2\text{N-Cr(III)}$ by chitosan.

Quantum theory of atoms in molecules

In order to explain the stability of the proposals, QTAIM calculations were performed. In fact, the electron distribution

analysis of a molecule is a promising starting point for the obtention of a chemical view of a molecule or an aggregate of molecules. QTAIM and NBO calculations are very important in an attempt to understand the nature of the chemical bond (for example, if the bond is covalent, partially covalent or non-covalent). Figure 7 shows proposal 2 as an illustrative example for this type of calculation. The other proposals follow a similar reasoning.

In order to explain the stability of proposal 3a, the results of the most stable proposal were compared with the initial compound (chitosan-Fe). By the criteria proposed by Koch and Popelier (1995), it is possible to observe the formation of hydrogen bonds; this criterion takes into account a hydrogen atom that is not interacting with the other atoms of the system. Thus, according to Koch and Popelier (1995), if hydrogen bonding occurs, an increase in $q(\Omega)$ and $E(\Omega)$, as well as a decrease in $V(H)$ and $M_1(H)$, must be observed (Table 6). Therefore, it is possible to note that the structure of chitosan-Fe does not meet the proposed criteria. As a consequence, the most stable proposal (proposal 3a) meets this criterion well. In Fig. 7, the atom marked yellow was selected for the analysis of the hydrogen bond.

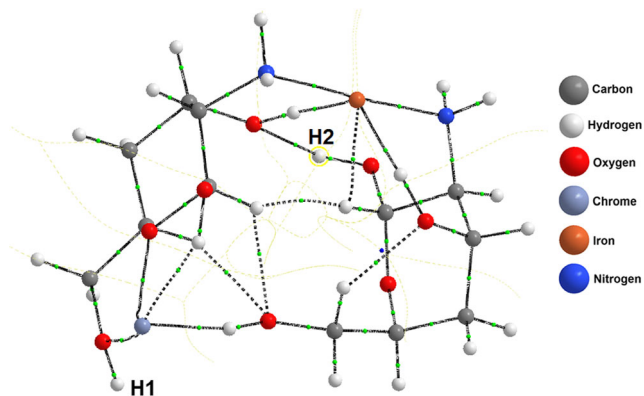


Fig. 7 Critical binding points (BCP and RCP) for proposal 2

Table 6 Additional atomic properties obtained by QTAIM calculations for atoms bound to hydrogen (in au)

Proposal	$q(H)$	$M_1(H)$	$V(H)$	$E(H)$
Chitosan-Fe				
$I_{H(OH)}$	+ 0.606029	+ 0.129206	+ 19.238196	+ 0.606029
$H_{IH(a)...O(a)}$	+ 0.573484	+ 0.125432	+ 16.149724	+ 0.573484
Proposal 3a				
$I_{H(OH)}$	+ 0.007659	+ 0.169859	+ 50.850527	- 0.620820
$H_{IH(a)...O(a)}$	+ 0.548286	+ 0.135135	+ 16.929473	- 0.380612

Conclusions

The CT-Fe hybrid composite was distinguished from the beads formed by pure CT, since it presented a highly rough and irregular morphology, besides high surface area, which positively contributes to the optimization of Cr(VI) removal by statistical design.

The statistical analysis central composite design indicated that all evaluated variables were significant (pH, concentration of chromium ions, adsorbent mass, and Fe(II) content in the beads) and showed an effect on aqueous Cr(VI) removal capacity. The pH was the most important parameter, indicating that the adsorption process was more favorable at acidic pH. As observed and discussed in this study, the combination between pH and concentration of chromium ions was extremely relevant for the efficiency of the reaction. Therefore, the statistical analysis applied to the evaluated parameters is adequate, allowing, in addition to choosing the best conditions for chromium removal, to work in future applications that are within the limits established in this study, together with the operational simplicity coming from the statistical design.

The optimum conditions of the parameters influenced the removal capacity of chromium ions, and the combination between them was important for favoring the adsorption kinetics. The pseudo-second-order kinetic model, the intraparticle diffusion model, and double-exponential models best fit the experimental data, indicating that the adsorption process follows by chemical interactions and occurs in two stages: firstly, the electrostatic attraction of the anionic form of chromium by the adsorbent CT-Fe, and chromium is then reduced and adsorbed onto the organic matrix of the composite.

The theoretical calculations are in agreement with the experimental results, in which the structure of CT-Fe-Cr(III) is more thermodynamically favorable than the proposed reactions with Cr(VI). It was also observed that, in the reaction mechanism, there is no competition of Fe(II) with Cr(III) and Cr(VI) at the available chitosan sites.

Acknowledgements The authors would like to thank CAPES, FAPEMIG, CNPq, the Postgraduate Program in Agrochemistry/UFLA, and Rede Mineira de Química.

References

APHA (2012) Standard methods for the examination of water and wastewater, 21st edn. American Public Health Association, Washington

Ashraf A, Bibi I, Niazi NK, Ok YS, Murtaza G, Shahid M, Kunhikrishnan A, Li DW, Mahmood T (2017) Chromium(VI) sorption efficiency of acid-activated banana peel over organo-montmorillonite in aqueous solutions. *Int J Phytoremediation* 19: 605–613. <https://doi.org/10.1080/15226514.2016.1256372>

Beheshti H, Irani M, Hosseini L, Rahimi A, Aliabadi M (2016) Removal of Cr (VI) from aqueous solutions using chitosan/MWCNT/Fe3O4

composite nanofibers-batch and column studies. *Chem Eng J* 284: 557–564. <https://doi.org/10.1016/j.cej.2015.08.158>

Bhatti IA et al (2017) Chromium adsorption using waste tire and conditions optimization by response surface methodology. *J Environ Chem Eng* 5(3):2740–2751. <https://doi.org/10.1016/j.cej.2015.08.158>

Bibi I, Niazi NK, Choppala G, Burton ED (2018) Chromium(VI) removal by siderite (FeCO₃) in anoxic aqueous solutions: an X-ray absorption spectroscopy investigation. *Sci Total Environ* 640:1424–1431. <https://doi.org/10.1016/j.scitotenv.2018.06.003>

Boyd GE, Adamson AW, Myers LS (1947) The exchange adsorption of ions from aqueous solutions by organic zeolites 2. *J Am Chem Soc* 69:2836–2848

Bozorgi M, Abbasizadeh S, Samani F, Mousavi SE (2018) Performance of synthesized cast and electrospun PVA/chitosan/ZnO–NH₂ nano-adsorbents in single and simultaneous adsorption of cadmium and nickel ions from wastewater. *Environ Sci Pollut Res* 25:17457–17472. <https://doi.org/10.1007/s11356-018-1936-z>

Branca C, D'Angelo G, Crupi C, Khouzami K, Rifici S, Ruello G, Wanderlingh U (2016) Role of the OH and NH vibrational groups in polysaccharide-nanocomposite interactions: a FTIR-ATR study on chitosan and chitosan/clay films. *Polymer* 99:614–622. <https://doi.org/10.1016/j.polymer.2016.07.086>

Buerge IJ, Hug SJ (1999) Influence of mineral surfaces on Chromium(VI) reduction by Iron(II). *Environ Sci Technol* 33(23):4285–4291. <https://doi.org/10.1021/es981297s>

Chagas PMB, Torres JA, Silva MC, Correa AD (2015) Immobilized soybean hull peroxidase for the oxidation of phenolic compounds in coffee processing wastewater. *Int J Biol Macromol* 81:568–575. <https://doi.org/10.1016/j.ijbiomac.2015.08.061>

Chagas PMB, de Carvalho LB, Caetano AA, Nogueira FGE, Corrêa AD, Guimarães I d R (2018) Nanostructured oxide stabilized by chitosan: hybrid composite as an adsorbent for the removal of chromium (VI). *J Environ Chem Eng* 6(1):1008–1019. <https://doi.org/10.1016/j.jece.2018.01.026>

Chiron N, Guilet R, Deydier E (2003) Adsorption of Cu(II) and Pb(II) onto a grafted silica: isotherms and kinetic models. *Water Res* 37: 3079–3086. [https://doi.org/10.1016/S0043-1354\(03\)00156-8](https://doi.org/10.1016/S0043-1354(03)00156-8)

Choi C, Nam JP, Nah JW (2016) Application of chitosan and chitosan derivatives as biomaterials. *J Ind Eng Chem* 33:1–10. <https://doi.org/10.1016/j.jiec.2015.10.028>

Conselho Nacional do Meio Ambiente – CONAMA (Brasil) (2011) Resolução n° 430 que altera a resolução n° 537, de 13 de maio de 2011. Dispõe sobre a classificação dos corpos d'água e diretrizes ambientais para o seu enquadramento, bem como estabelece as condições e padrões de lançamento de efluentes, dá outras Providências. *Diário Oficial da República Federativa do Brasil*, Brasília, DF, 18 mar. seção 3, p. 7

Cornell RM, Schwertmann U (2003) The iron oxides, 3th edn. J. Wiley-VCH, New York

Cunha GD et al (2016) Recycling of chromium wastes from the tanning industry to produce ceramic nanopigments. *Green Chem* 18(19): 5342–5356. <https://doi.org/10.1039/C6GC01562J>

Dinker MK, Kulkarni PS (2015) Recent advances in silica-based materials for the removal of hexavalent chromium: a review. *J Chem Eng Data* 60(9):2521–2540. <https://doi.org/10.1021/acs.jced.5b00292>

Gyliene O et al (2014) Influence of dissolved oxygen on Fe(II) and Fe(III) sorption onto chitosan. *Colloids Surf A Physicochem Eng Asp* 461: 151–157. <https://doi.org/10.1016/j.colsurfa.2014.07.027>

Haldorai Y, Rengaraj A, Ryu T, Shin J, Huh YS, Han YK (2015) Response surface methodology for the optimization of lanthanum removal from an aqueous solution using a Fe₃O₄/chitosan nanocomposite. *Mater Sci Eng B* 195:20–29. <https://doi.org/10.1016/j.mseb.2015.01.006>

Hao C, Yang Y, Shen Y, Feng F, Wang X, Zhao Y, Ge C (2016) Liquid phase-based ultrasonic-assisted synthesis of G-ZnO nanocomposites

- and its sunlight photocatalytic activity. *Mater Des* 89:864–871. <https://doi.org/10.1016/j.matdes.2015.10.041>
- Hua M, Zhang SJ, Pan BC, Zhang WM, Lv L, Zhang QX (2012) Heavy metal removal from water/wastewater by nanosized metal oxides: a review. *J Hazard Mater* 211:317–331. <https://doi.org/10.1016/j.jhazmat.2011.10.016>
- Keith TA (2010) Aimall (version 10.05.04), TKGristmill software, Overland Park KS. <http://aim.tkgristmill.com/>
- Kim MK, Sundaram KS, Iyengar GA, Lee KP (2015) A novel chitosan functional gel included with multiwall carbon nanotube and substituted polyaniline as adsorbent for efficient removal of chromium ion. *Chem Eng J* 267:51–64. <https://doi.org/10.1016/j.cej.2014.12.091>
- Koch U, Popelier PLA (1995) Characterization of C-H-O hydrogen-bonds on the basis of the charge-density. *J Phys Chem* 99:9747–9754. <https://doi.org/10.1021/j100024a016>
- Lee CG, Lee S, Park JA, Park C, Lee SJ, Kim SB, An B, Yun ST, Lee SH, Choi JW (2017) Removal of copper, nickel and chromium mixtures from metal plating wastewater by adsorption with modified carbon foam. *Chemosphere* 166:203–211. <https://doi.org/10.1016/j.chemosphere.2016.09.093>
- Li LL, Fan LL, Sun M, Qiu HM, Li XJ, Duan HM, Luo CN (2013) Adsorbent for chromium removal based on graphene oxide functionalized with magnetic cyclodextrin-chitosan. *Colloids Surf B: Biointerfaces* 107:76–83. <https://doi.org/10.1016/j.colsurfb.2013.01.074>
- Lingamdinne LP, Chang YY, Yang JK, Singh J, Cho EH, Shiratani M, Koduru JR, Attri P (2017) Biogenic reductive preparation of magnetic inverse spinel iron oxide nanoparticles for the adsorption removal of heavy metals. *Chem Eng J* 307:74–84. <https://doi.org/10.1016/j.cej.2016.08.067>
- Lu J, Xu K, Yang J, Hao Y, Cheng F (2017) Nano iron oxide impregnated in chitosan bead as a highly efficient sorbent for Cr(VI) removal from water. *Carbohydr Polym* 173:28–36. <https://doi.org/10.1016/j.carbpol.2017.05.070>
- Lv XS, Xu J, Jiang GM, Xu XH (2011) Removal of chromium(VI) from wastewater by nanoscale zero-valent iron particles supported on multiwalled carbon nanotubes. *Chemosphere* 85:1204–1209. <https://doi.org/10.1016/j.chemosphere.2011.09.005>
- Madala S, Nadavala SK, Vudagandla S, Boddu VM, Abburi K (2017) Equilibrium, kinetics and thermodynamics of Cadmium (II) biosorption on to composite chitosan biosorbent. *Arab J Chem* 10: S1883–S1893. <https://doi.org/10.1016/j.arabjc.2013.07.017>
- Neese F (2012) The ORCA program system. *Wiley Interdiscip Rev Comput Mol Sci* 233:73–78. <https://doi.org/10.1002/wcms.81>
- Neto BB, Scarminio IS, Bruns RE (2010) Como Fazer Experimentos. Editora Bookman, 4ª Edição
- Nunes CA, Freitas MP, Pinheiro ACM, Bastos SC (2012) Chemoface: a novel free user-friendly interface for chemometrics. *J Braz Chem Soc* 23:2003–2010. <https://doi.org/10.1590/S0103-50532012005000073>
- Pasquini C (2003) Near infrared spectroscopy: fundamentals, practical aspects and analytical applications. *J Braz Chem Soc* 14:198–219. <https://doi.org/10.1590/S0103-50532003000200006>
- Prado C, Ponce SC, Pagano E, Prado FE, Rosa M (2016) Differential physiological responses of two *Salvinia* species to hexavalent chromium at a glance. *Aquat Toxicol* 175:213–221. <https://doi.org/10.1016/j.aquatox.2016.03.027>
- Prahas D, Kartika Y, Indraswati N, Ismadji S (2008) Activated carbon from jackfruit peel waste by H₃PO₄ chemical activation: pore structure and surface chemistry characterization. *Chem Eng J* 140:32–42. <https://doi.org/10.1016/j.cej.2007.08.032>
- Qin JX, Tan P, Jiang Y, Liu XQ, He QX, Sun LB (2016) Functionalization of metal-organic frameworks with cuprous sites using vapor-induced selective reduction: efficient adsorbents for deep desulfurization. *Green Chem* 18:3210–3215. <https://doi.org/10.1039/C6GC00613B>
- Rakkapao N, Vao-soongnern V, Masubuchi Y, Watanabe H (2011) Miscibility of chitosan/poly(ethylene oxide) blends and effect of doping alkali and alkali earth metal ions on chitosan/PEO interaction. *Polymer* 52:2618–2627. <https://doi.org/10.1016/j.polymer.2011.03.044>
- Rossi LM, Costa NJS, Silva FP, Wojcieszak R (2014) Magnetic nanomaterials in catalysis: advanced catalysts for magnetic separation and beyond. *Green Chem* 16:2906–2933. <https://doi.org/10.1039/C4GC00164H>
- Sahu PK, Sahu PK, Gupta SK, Agarwal DD (2014) Chitosan: an efficient, reusable, and biodegradable catalyst for green synthesis of heterocycles. *Ind Eng Chem Res* 53:2085–2091. <https://doi.org/10.1021/ie402037d>
- Sampaio CD, Frota LS, Magalhaes HS, Dutra LMU, Queiroz DC, Araujo RS, Becker H, de Souza JRR, Ricardo N, Trevisan MTS (2015) Chitosan/mangiferin particles for Cr(VI) reduction and removal. *Int J Biol Macromol* 78:273–279. <https://doi.org/10.1016/j.ijbiomac.2015.03.038>
- Sen Gupta S, Bhattacharyya KG (2011) Kinetics of adsorption of metal ions on inorganic materials: a review. *Adv Colloid Interf Sci* 162: 39–58. <https://doi.org/10.1016/j.cis.2010.12.004>
- Shahid M, Shamsad S, Rafiq M, Khalid S, Bibi I, Niazi NK, Dumat C, Rashid MI (2017) Chromium speciation, bioavailability, uptake, toxicity and detoxification in soil-plant system: a review. *Chemosphere* 178:513–533. <https://doi.org/10.1016/j.chemosphere.2017.03.074>
- Shekari H, Sayadi MH, Rezaei MR, Allahresani A (2017) Synthesis of nickel ferrite/titanium oxide magnetic nanocomposite and its use to remove hexavalent chromium from aqueous solutions. *Surf and Interf* 8:199–205. <https://doi.org/10.1016/j.surfin.2017.06.006>
- Sikder MT, Mihara Y, Islam MS, Saito T, Tanaka S, Kurasaki M (2014) Preparation and characterization of chitosan-caboxymethyl-beta-cyclodextrin entrapped nanozero-valent iron composite for Cu (II) and Cr (IV) removal from wastewater. *Chem Eng J* 236:378–387. <https://doi.org/10.1016/j.cej.2013.09.093>
- Simonin JP (2016) On the comparison of pseudo-first order and pseudo-second order rate laws in the modeling of adsorption kinetics. *Chem Eng J* 300:254–263. <https://doi.org/10.1016/j.cej.2016.04.079>
- Singh N, Ahmad A (2010) Spectrophotometric and spectroscopic studies of charge transfer complex of 1-Naphthylamine as an electron donor with picric acid as an electron acceptor in different polar solvents. *J Mol Struct* 977:197–202. <https://doi.org/10.1016/j.molstruc.2010.05.032>
- Su CM (2017) Environmental implications and applications of engineered nanoscale magnetite and its hybrid nanocomposites: a review of recent literature. *J Hazard Mater* 322:48–84. <https://doi.org/10.1016/j.jhazmat.2016.06.060>
- Tahar LB, Oueslati MH, Abualreish MJA (2018) Synthesis of magnetite derivatives nanoparticles and their application for the removal of chromium (VI) from aqueous solutions. *J Colloid Interface Sci* 512:115–126. <https://doi.org/10.1016/j.jcis.2017.10.044>
- Talebi M, Abbasizadeh S, Keshtkar AR (2017) Evaluation of single and simultaneous thorium and uranium sorption from water systems by an electrospun PVA/SA/PEO/HZSM5 nanofiber. *Process Saf Environ Prot* 109:340–356. <https://doi.org/10.1016/j.psep.2017.04.013>
- Tehrani MM, Abbasizadeh S, Alamdari A, Mousavi SE (2017) Prediction of simultaneous sorption of copper(II), cobalt(II) and zinc(II) contaminants from water systems by a novel multi-functionalized zirconia nanofiber. *Desalin Water Treat* 62:403–417. <https://doi.org/10.5004/dwt.2017.20135>
- Thommes M, Kaneko K, Neimark AV, Olivier JP, Rodriguez-Reinoso F, Rouquerol J, Sing KSW (2015) Physisorption of gases, with special reference to the evaluation of surface area and pore size distribution

- (IUPAC Technical Report). *Pure Appl Chem* 87:1051–1069. <https://doi.org/10.1515/pac-2014-1117>
- Vieira RS, Meneghetti E, Baroni P, Guibal E, de la Cruz VMG, Caballero A, Rodriguez-Castellon E, Beppu MM (2014) Chromium removal on chitosan-based sorbents - An EXAFS/XANES investigation of mechanism. *Mater Chem Phys* 146:412–417. <https://doi.org/10.1016/j.matchemphys.2014.03.046>
- Wang KP, Liu Q (2014) Chemical structure analyses of phosphorylated chitosan. *Carbohydr Res* 386:48–56. <https://doi.org/10.1016/j.carres.2013.12.021>
- Weber WJ, Morris JC (1963) Kinetics of adsorption on carbon from solution. *J Sanit Eng Div* 89:31–60
- World Health Organization (WHO) (2004) Organization, Guidelines for drinking — water quality, 3rd edn. WHO, Geneva, p 515
- Wibowo E, Rokhmat M, Khairurrijal S, Abdullah M (2017) Reduction of seawater salinity by natural zeolite (Clinoptilolite): adsorption isotherms, thermodynamics and kinetics. *Desalination* 409:146–156. <https://doi.org/10.1016/j.desal.2017.01.026>
- Wu YH, Ming Z, Yang SX, Fan Y, Fang P, Sha HT, Cha LG (2017) Adsorption of hexavalent chromium onto Bamboo Charcoal grafted by Cu²⁺-N-aminopropylsilane complexes: optimization, kinetic, and isotherm studies. *J Ind Eng Chem* 46:222–233. <https://doi.org/10.1016/j.jiec.2016.10.034>
- Xiao YZ, Liang HF, Wang ZC (2013) MnFe₂O₄/chitosan nanocomposites as a recyclable adsorbent for the removal of hexavalent chromium. *Mater Res Bull* 48:3910–3915. <https://doi.org/10.1016/j.materresbull.2013.05.099>
- Yan H, Yang H, Li AM, Cheng RS (2016) pH-tunable surface charge of chitosan/graphene oxide composite adsorbent for efficient removal of multiple pollutants from water. *Chem Eng J* 284:1397–1405. <https://doi.org/10.1016/j.cej.2015.06.030>
- Yao W, Rao PH, Lo IMC, Zhang WQ, Zheng WR (2014) Preparation of cross-linked magnetic chitosan with quaternary ammonium and its application for Cr(VI) and P(V) removal. *J Environ Sci* 26:2379–2386. <https://doi.org/10.1016/j.jes.2014.03.005>
- Ye Y, Jiang Z, Xu Z, Zhang X, Wang D, Lv L, Pan B (2017) Efficient removal of Cr(III)-organic complexes from water using UV/Fe(III) system: negligible Cr(VI) accumulation and mechanism. *Water Res* 126:172–178. <https://doi.org/10.1016/j.watres.2017.09.021>
- Zhang L, Luo HJ, Liu PP, Fang W, Geng JJ (2016) A novel modified graphene oxide/chitosan composite used as an adsorbent for Cr(VI) in aqueous solutions. *Int J Biol Macromol* 87:586–596. <https://doi.org/10.1016/j.ijbiomac.2016.03.027>
- Zhu GC, Liu JF, Yin J, Li ZW, Ren BZ, Sun YJ, Wan P, Liu YS (2016) Functionalized polyacrylamide by xanthate for Cr(VI) removal from aqueous solution. *Chem Eng J* 288:390–398. <https://doi.org/10.1016/j.cej.2015.12.043>
- Zhurko GA, Zhurko DA (2015) Chemcraft program, Academic version. <http://www.chemcraftprog.com>

Publisher's note Springer Nature remains neutral with regard to jurisdictional claims in published maps and institutional affiliations.